A Multiaxial Fatigue Model for Steel Joints

S.A.Sudath C. Siriwardane,
Department of Mechanical, Structural Engineering and Materials Science,
University of Stavanger, Norway
(sasc.siriwardane@uis.no)

P.B.R. Dissanayake
Department of Civil Engineering, University of Peradeniya, Sri Lanka
(ranjith@civil.pdn.ac.lk)

Abstract

This paper presents a new model to estimate multiaxial high cycle fatigue life of steel joints, when it is subjected to variable amplitude proportional loadings. The considered failure mechanism of proposed model is in mesoscopic scale (grain scale). The model mainly consists of a new damage indicator, which gives a better prediction to fatigue life than existing fatigue models. The verification of the proposed fatigue model is performed by comparing the experimental fatigue lives with theoretical predictions. It is shown that the proposed multiaxial fatigue model gives much more realistic fatigue life than previous models in both variable amplitude and random loading conditions. Finally, proposed model is applied to estimate fatigue life of a steel joint and associated procedure is clearly indicated.

Keywords: High cycle fatigue, Meso-plastic strain; Multiaxial stress; Steel Joints

1. Introduction

The effect of stress concentration in connections between primary members of structures was found to be one of the main reasons for fatigue damage (Fisher et al., 1984; Imam et al., 2005). Most of these connections are subjected to multiaxial fatigue in both high cycle and low cycle ranges. In case of high cycle fatigue, the equivalent effective stress with Miner's rule is the most popular multiaxial fatigue criterion in service life estimation of structures (Imam et al., 2005 & 2007; Suresh, 1998). However under many variable amplitude-loading conditions, Miner's predictions have been found to be unreliable since it does not properly take into account the loading sequence (Mesmeque et al., 2005). Recently, a number of damage models have been proposed to capture the loading sequence effect of variable amplitude loads more precisely.

The scale of metal grains of a metallic aggregate is generally defined to be within the mesoscopic scale (grain scale). Many of the more precise high cycle fatigue theories involve grain scale than macroscopic scale. In the high cycle fatigue region, some grains undergo local plasticity while the rest of the matrix behaves elastically. Recently, one mesoscopic scale fatigue model (Jabbado et al. 2008) was developed to obtain more precise estimation to multiaxial fatigue. However, experimental comparisons of this theory (model) have exhibited a certain amount of deviation for multiaxial fatigue life due to variable amplitude loading conditions since the considered damage law is Miner's rule.

Therefore the main objective of this paper is to propose a new mesoscopic scale (grain scale) fatigue model to obtain a more precise estimation to multiaxial high cycle fatigue life for variable amplitude or random proportional loading. The accumulated inelastic meso-strain is considered as the damage variable in this model, and a new damage indicator is defined as an alternative to the damage factor of the previous model. Initially chapter describes the existing multiaxial high cycle fatigue models and their shortcomings. Then, the chapter describes the new fatigue model. The verification of the proposed fatigue model is performed by comparing the experimental fatigue lives with theoretical predictions. The proposed model is applied to estimate the fatigue life of a steel joint and obtained results are compared with previous estimations based on other known models. Finally, it is shown that the proposed multiaxial fatigue model gives a much more realistic fatigue life to variable amplitude proportional loading situation where detailed stress histories are known.

2. Proposed fatigue model

This section proposes a new high cycle fatigue model for multiaxial variable amplitude loading. The considered failure mechanism (damage process) is in mesoscopic scale and accumulated inelastic meso-strain is considered as the damage variable. Initially, the relation to obtain the accumulated plastic strain per stabilized cycle is indicated. Then the section describes mesoscopic law of fatigue law for constant amplitude loading and newly proposed damage indicator respectively. A model parameter determination procedure is also clearly stated at end of the section.

2.1 Accumulated plastic meso-strain per stabilized cycle

Considering the mesoscopic scale elasto-plastic behavior, accumulated plastic meso-strain (ε_s^{pc}) per stabilized cycle for constant amplitude proportional loading is found to be (Jabbado et al. 2008).

$$\varepsilon_s^{pc} = \frac{4}{\sqrt{3}} \frac{2k^* - k_{\max} - k_{\min}}{c} \tag{1}$$

where $c = b + 2\eta$. The b and η are the mesoscopic linear hardening modulus and the shear modulus respectively. The k^* is the radius of the smallest hypersphere which contains the entire history of the macroscopic deviatoric stress amplitude of the stabilized cycle ($\sigma'_{ij,a}$) as follows,

$$k^* = \sqrt{\tfrac{1}{2}\sigma'_{ij,a}\sigma'_{ij,a}} \tag{2}$$

The $k_{\max}$ and $k_{\min}$ are the maximum and the minimum values of mesoscopic yield stresses that can be reached during the loading cycle. The instantaneous hydrostatic stress does not have the same effect in tension as in compression. Generally tension progressively opens the microcracks, while compression closes the microcracks and therefore has less effect on damage. Therefore mesoscopic yield stress depends on the instantaneous hydrostatic stress which has similar value of macroscopic hydrostatic stress when simplified macro-meso relationship is adopted . Hence the maximum and the minimum values of mesoscopic yield stresses are derived as,

$$k_{\min} = \beta - \alpha p_a \text{ and } k_{\max} = \beta + \gamma p_a \tag{3}$$

where p_a is the macroscopic hydrostatic stress amplitude of a stabilized cycle. The α, β and γ are material parameters and these have to be determined using two fatigue limits (for example torsion and bending fatigue limits) and one *S-N* curve of particular material. The determination procedure has been described in detail at the section 2.4

2.2 Mesoscopic law of fatigue life for constant amplitude loadings

The mesoscopic law of fatigue life for constant amplitude proportional loading situation is described as a power relationship combining the accumulated plastic meso-strain per stabilized cycle (ε_s^{pc}) with the number of cycles to crack nucleation N (Jabbado et al. 2008).

$$N = A(\varepsilon_s^{pc})^{-\xi} \tag{4}$$

where ξ and A are material parameters to be determined from fatigue tests.

2.3 Proposed damage indicator for variable amplitude loading

The hypothesis behind this fatigue law is that if the physical state of damage is the same, then fatigue life depends only on the loading condition. Suppose a component is subjected to a certain accumulated plastic meso-strain $(\varepsilon_s^{pc})_i$ per stabilized cycle of n_i number of cycles at load level i, N_i is the fatigue life (number of cycles to crack nucleation) corresponding to $(\varepsilon_s^{pc})_i$ (Fig.

1). Hence, the residual life at load level i can be obtained as (N_i–n_i). The accumulated plastic

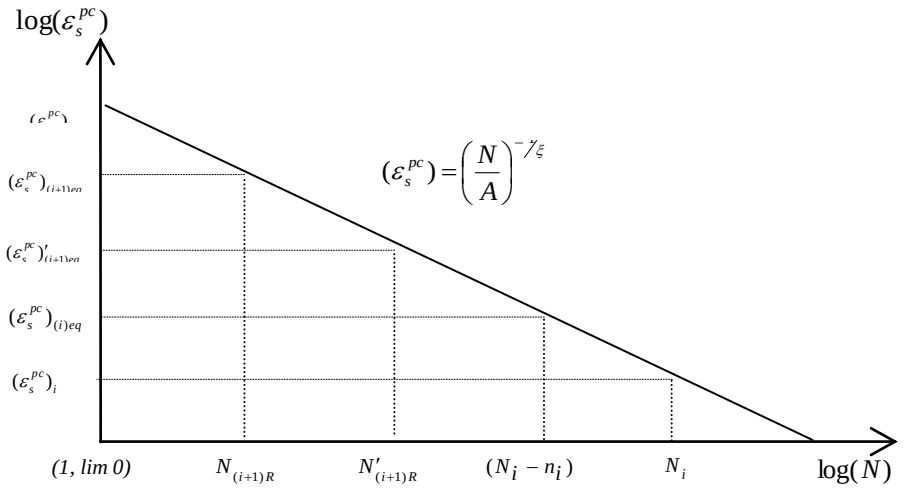

Figure 1: Schematic representation of mesoscopic law of fatigue life for constant amplitude loading

meso-strain $(\varepsilon_s^{pc})_{(i)eq}$, which corresponds to the failure life (N_i–n_i) is named as i^{th} level damage accumulated plastic meso-strain. Hence, the new damage indicator, D_i is stated as,

$$D_i = \frac{(\varepsilon_s^{pc})_{(i)eq} - (\varepsilon_s^{pc})_i}{(\varepsilon_s^{pc})_u - (\varepsilon_s^{pc})_i} \tag{5}$$

where $(\varepsilon_s^{pc})_u$ is the intercept in Fig. 1 with the ordinate at one-quarter of first fatigue cycle, i.e. accumulated plastic meso-strain corresponding to ductile farcture (Suresh, 1998). Here it is assumed that tensile fracture is initiated at the peak positive value of first cycle of the applied stress. Further it considered that the simple tensile test represents one-quarter of a single completely reversed fatigue cycle.

Assuming the end of i^{th} loading level damage D_i has been accumulated (occurred) due to the effect of $(\varepsilon_s^{pc})_{i+1}$ loading cycles, the damage is transformed to load level $i+1$ as bellow.

$$D_i = \frac{(\varepsilon_s^{pc})'_{(i+1)eq} - (\varepsilon_s^{pc})_{i+1}}{(\varepsilon_s^{pc})_u - (\varepsilon_s^{pc})_{i+1}} \tag{6}$$

The $(\varepsilon_s^{pc})'_{(i+1)eq}$ is damage equivalent accumulated plastic meso-strain at loading level $i+1$ and it can be calculated from Eq. (6) as,

$$(\varepsilon_s^{pc})'_{(i+1)eq} = D_i[(\varepsilon_s^{pc})_u - (\varepsilon_s^{pc})_{i+1}] + (\varepsilon_s^{pc})_{i+1} \tag{7}$$

Thus the corresponding equivalent number of cycles to failure $N'_{(i+1)R}$ can be obtained from the Eq. (4) as shown in Fig. 1. The $(\varepsilon_s^{pc})_{i+1}$ is the accumulated plastic meso-strain at the level $i+1$ and supposing that it is subjected to $n_{(i+1)}$ number of cycles, then the corresponding residual life at load level $i+1$, $N_{(i+1)R}$ is calculated as,

$$N_{(i+1)R} = N'_{(i+1)R} - n_{(i+1)} \tag{8}$$

Hence damage accumulated plastic meso-strain $(\varepsilon_s^{pc})_{(i+1)eq}$, which corresponds to $N_{(i+1)R}$ at load level *i+1*, can be obtained from the Eq. (4) as shown in Fig. 1. Then the cumulative damage at the end of load level *i+1* is defined as,

$$D_{(i+1)} = \frac{(\varepsilon_s^{pc})_{(i+1)eq} - (\varepsilon_s^{pc})_{i+1}}{(\varepsilon_s^{pc})_u - (\varepsilon_s^{pc})_{i+1}} \tag{9}$$

At the first cycle the damage accumulated plastic meso-strain $(\varepsilon_s^{pc})_{(i)eq}$ is equal to $(\varepsilon_s^{pc})_i$ and the corresponding damage indicator becomes D_i=0. Similarly at the last cycle, the damage indicator becomes D_i=1 when $(\varepsilon_s^{pc})_{(i)eq}$ is equal to $(\varepsilon_s^{pc})_u$. Therefore, the damage indicator is normalized to one (D_i=1) at the fatigue failure of the material. Hence, the above procedure is followed until D_i=1. Here, the defined fatigue failure is time taken for initiation of crack at the location of maximum stress of the structural component. In the case of railway bridge components, it can probably be taken as the time taken for initiation of crack near a connection.

2.4 Determination of model parameters

The mesoscopic law for constant amplitude loading (Eq. (4)) depends on two material parameters ξ and *A*. The accumulated plastic meso-strain (ε_s^{pc}) per stabilized cycle in Eq. (1) depends on four parameters α, β, γ and *c*. However all six parameters are similar to previous mesoscopic model (Jabbado et al. 2008). Therefore, the determination method is also similar to the previous model and those are identified by using two fatigue limits (for example torsion and bending fatigue limits) and one *S-N* curve.

In the fully reversed torsion fatigue limit, the accumulated plastic meso-strain per stabilized cycle is zero ($\varepsilon_s^{pc} = 0$), as the grain asymptotically behaves elastically. Following the Eq. (2), the radius of the smallest hypersphere (k^*) can be derived as the value of torsion fatigue limit (t_{-1}). Since the material is in pure torsion, the macroscopic hydrostatic stress amplitude is also zero ($p_a = 0$). Substituting these values to Eq. (1), parameter β can be obtained as,

$$\beta = t_{-1} \tag{10}$$

Same as above, in the fully reversed bending fatigue limit (f_{-1}), the accumulated plastic meso-strain per stabilized cycle is zero ($\varepsilon_s^{pc} = 0$), as the grain asymptotically behaves elastically. Following the Eq. (2), the radius of the smallest hypersphere is derived as $k^* = f_{-1}/\sqrt{3}$. The macroscopic hydrostatic stress amplitude can be obtained as, $p_a = f_{-1}/3$. Substituting these values to Eq. (1), following relation of parameters α, β and γ can be derived.

$$\alpha - \gamma = 2\left(\frac{3\beta}{f_{-1}} - \sqrt{3}\right) \tag{11}$$

In the finite life domain of fully reversed *S-N* curve, the accumulated plastic meso-strain (ε_s^{pc}) per stabilized cycle can be obtained from Eq. (1) as,

$$\varepsilon_s^{pc} = \frac{2\frac{f}{\sqrt{3}} - 2\beta + \frac{f}{3}(\alpha - \gamma)}{c} \times \frac{4}{\sqrt{3}} \tag{12}$$

The Eq. (13) depends on the all six parameters. The best values of these parameters are determined by minimizing the error between the calculated (N_{cal}) and experimental ($N_{\exp}$) fatigue lives. To find best values, an optimization problem has to be performed by considering objective function as,

$$F_{Objective} = \sum abs\left(\frac{N_{cal}}{N_{\exp}} - 1\right) \tag{14}$$

and constrains as the Eq. (10) & (11). To solve this problem efficiently, authors recommend the use the genetic algorithm employed toolbox in Mathlab Program.

3. Verification of proposed fatigue model

In favour of verification, the models predicted fatigue lives were compared with previously proposed models and the experimentally observed fatigue lives of some of fatigue tests under both variable amplitude and random loading situations.

3.1 Comparison with experimental life under variable amplitude load

In this section, the multiaxial fatigue test results of two materials are compared with the theoretically predicted fatigue lives under variable amplitude loading situations. The two materials are 18G2A and 10HNAP steels. The first material is a low alloy high-strength steel for building welded structures. The other material is a low-alloy structural steel of higher resistance to atmospheric corrosion. The tests were performed in the high cycle fatigue region under variable amplitude combined bending and torsion loading. Histories of bending and torsion moments have been independently generated. Then the nominal normal and shear stress histories were obtained using the section modulus of bending and torsion (Marciniak et al., 2008). The obtained normal and shear stresses were both in-phase loading (proportional loading). The dominant loading frequency was 20 Hz. The time interval of loading repetition (duration of loading block) was equal to 2000 seconds. Fatigue tests were performed under two proportional loading combinations for the 18G2A steel. For the 10HNAP steel, three proportional loading combinations were tested. The fragments of normal and shear stress histories, obtained across the critical cross section during a selected loading combination are drawn in Fig. 2 to illustrate the variable amplitude nature of loading histories. The stress histories of all these proportional loading combinations exhibit nearly zero mean stress effect. This provides evidence to conclude that each loading cycle of entire history generate a stabilized mesoscopic stress/ strain cycle for all the combinations.

The partially known fully reversed tension-compression *S-N* curves and fatigue limits for tension-compression and torsion of above materials were obtained from different research papers (Korolczuk et al., 2005; Kluger et al., 2004). Using these data and following the guidelines given in section 2.4, a constrained minimization problem was performed to estimate the parameters $\alpha, \beta, \gamma, \xi$, c and A. The obtained values for $\alpha, \beta, \gamma, \xi$, c and A of 18G2A steel were 1.62, 170 MPa, 0.0841,0.9827, 49213 MPa and 987 respectively. The corresponding values for 10HNAP steel were 0.9016, 182 MPa, 0.0324, 0.9001, 48734 MPa and 1370

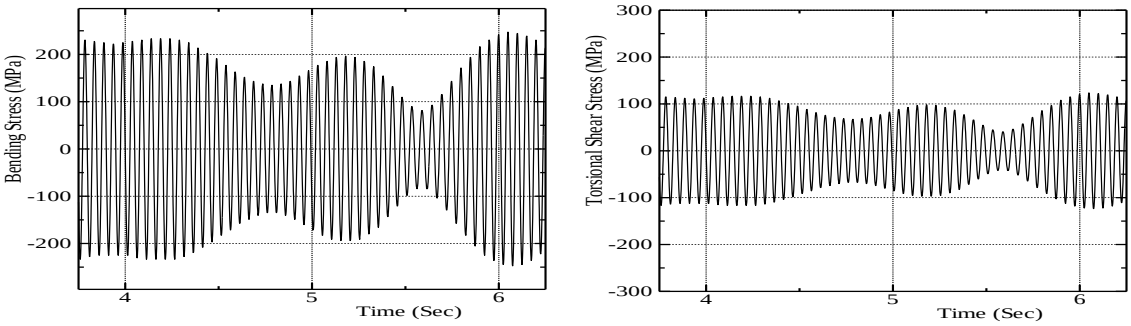

(a) (b)

Figure 2: Fragments of history of nominal stress for: (a) bending and (b) torsion

respectively. The proposed fatigue model is applied to obtain the theoretical fatigue life of each mentioned loading combinations. The comparisons between the calculated lives and the experimental results are shown Fig.3. In addition to this, experimental lives are compared with two previous theoretical approaches as shown in Fig.3. The first approach is based on equivalent effective stress with Miner's rule (Suresh, 1998). The second approach is based on previous mesoscopic approach (Jabbado et al., 2008). Finally Fig. 3 shows that there is better agreement between the values from the proposed model and the real fatigue life of these materials than the lives predicted by previous models. This verification reveals the validity of the proposed mesoscopic scale fatigue model in predicting the multiaxial fatigue life under variable amplitude proportional loading conditions.

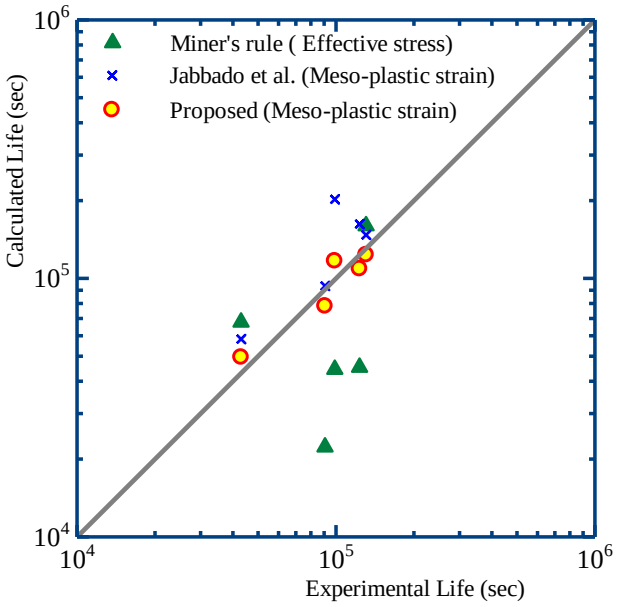

Figure 3: Comparison of calculated life versus experimental life

3.2 Comparison with experimental life under random load

The multiaxial fatigue test results under random loading of 10HNAP material are compared with the theoretically predicted fatigue lives in this section. The considered material is a low-alloy structural steel of higher resistance to atmospheric corrosion. The rounds specimens were tested in high cycle fatigue region under combination of proportional bending, $M_B(t)$, and torsional, $M_T(t)$, moments. The 14 specimens, which are subjected to $\alpha = \pi/4$ (i.e. $tg\alpha = M_T(t)/M_B(t)$), were selected for this comparison (Jabbado et al., 2008). The dominant sampling frequency of loading history was 266.67 Hz. The time interval of loading repetition (duration of loading block) was equal to 184.32 seconds. The proportional random histories of bending normal stress and torsional shear stress for these tests are obtained by multiplying the random loading sequence by loading factors corresponding to bending and torsion moments. The fragments of normal and shear stress histories, obtained across the critical cross section during a selected loading combination are drawn in Fig. 4 to illustrate the random nature of loading histories. The obtained stress histories are complex and also of irregular shape. These stresses should be reduced into a series of equivalent stabilized cycles (zero mean stress cycles) which give the same damage to the material. In order to achieve this goal, initially the famous rainflow cycle counting technique (Suresh, 1998) is used to identify the stress ranges and sequences of closed stress cycles (Suresh, 1998; Christ, 1996). Then modified Goodman relation (Suresh, 1998) is used to transfer these counted cycle to mean stress zero equivalent stabilized cycle.

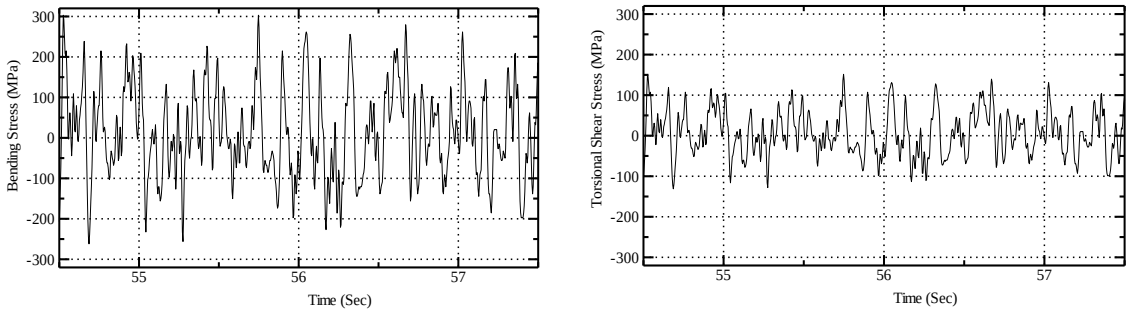

(a) (b)

Figure 4: Fragments of nominal stress history of multiaxial random loading test for: (a) bending and (b) torsion

The partially known fully reversed tension-compression *S-N* curves and fatigue limits for tension-compression and torsion of above materials were obtained from different research papers similar to section 3.1. Using these data and following the guidelines given in section 2.4, a constrained minimization problem was performed to estimate the parameters $\alpha, \beta, \gamma, \xi$, c and A. The obtained values for $\alpha, \beta, \gamma, \xi$, c and A of for 10HNAP steel were 0.9016, 182 MPa, 0.0324, 0.9001, 48734 MPa and 1370 respectively. The proposed fatigue model is applied to obtain the theoretical fatigue life of each mentioned loading combinations. The comparisons between the calculated lives and the experimental results are shown in Fig. 5. In addition to this,

experimental lives are compared with three previous theoretical approaches as shown in Fig. 5. The first approach is based on equivalent effective stress with Miner's rule (Suresh, 1998). The second approach is based on critical plane which is used to define an equivalent stress amplitude (Carpinteri et al., 2003). Here, the critical plane is determined from the weighted mean position of the principle stress directions. The last approach among the previous approaches is based on previous mesoscopic approach (Jabbado et al., 2008). Finally Fig.5 shows that there is better agreement between the values from the proposed model and the real fatigue life of these materials than the lives predicted by previous models. This verification reveals the validity of the proposed mesoscopic scale fatigue model in predicting the multiaxial fatigue life under random proportional loading conditions.

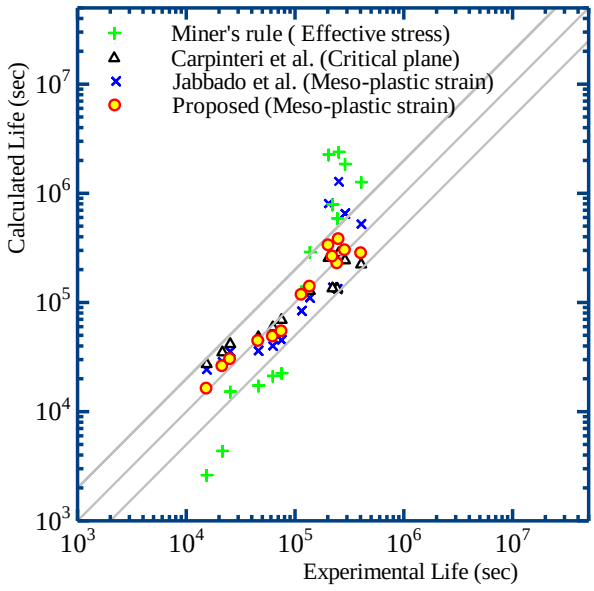

Figure 5: Comparison of calculated life versus experimental life

4. Application of proposed model to riveted connection

Fatigue life evaluation of a riveted joint (Fig. 6) is discussed in this section. The evaluations are especially based on secondary stresses, which are generated around the riveted connection due to stress concentration effect of primary stress.

4.1 Stress Analysis

The fatigue damage is evaluated based on the state of stress due to release of contact (tightness) of rivet while all the riveted locations have no clamping force. Therefore, a critical member without rivets can be considered to analyze biaxial state of stress (Fig. 7 (a)). The primary tensile stress history (Fig. 8) of the critical member, which has been obtained from measured strain histories at mid span of the member (Siriwardane et al. 2008), is applied on the bottom face (*ab* of Fig. 7(a)) as an uniform pressure. The position of the *ab* boundary of the sub-model was determined considering the distribution of far field primary stress of the member. The four-node shell elements were used for the finite element analysis. The actual air gap restraint conditions were considered in the model to represent unilateral contact between rivet and plate. The obtained maximum stress contours are shown in Fig. 7. This shows that stresses are operating well bellow the yield limit of the material and highly stressed locations (critical locations) are subjected to biaxial proportional state of stress. The principle stress variations versus the traffic sequence were obtained as shown in Fig.9. Assuming that single day traffic sequence (time table) is repeating every day, one day time history is considered as the loading block in this study.

Critical member

Figure 6. Considered joint

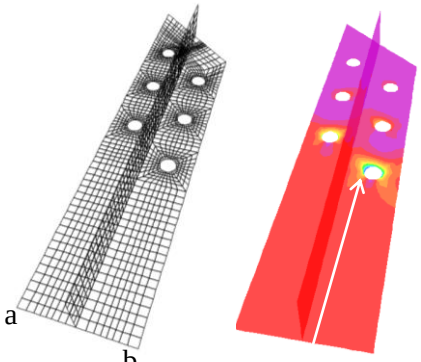

(a) (b)

Figure.7: Stress analysis: (a) FE mesh, (b) Maximum von Mises stress contour when all six rivets are active

4.2 Determination of model parameters

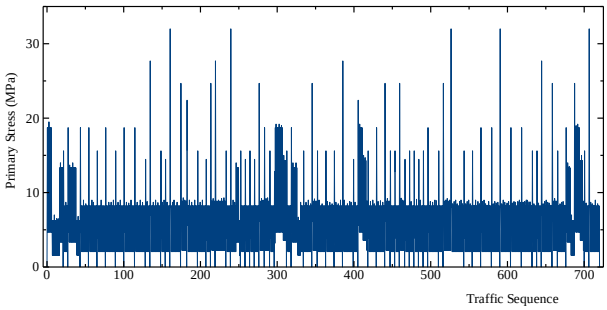

Figure 8. Primary stress variation of the member with traffic sequence per single day

The material of riveted member is Wrought iron and relevant design (mean minus two standard deviations) *S-N* curve, which represents low or no clamping force effect at the rivets, was obtained from the UK railway assessment code and previous paper (Railtrack 2001). The design reversed tension- compression fatigue limit was determined from above *S-N* curve corresponding to 10^8 failure number of cycles. Then, general relations between the fatigue limits of particular material was used to calculate fully reversed torsion fatigue limit of Wrought iron material (Troshchenko et al. 1975). Using these data and following the guidelines given in section 2.4, a constrained minimization problem was performed to estimate the parameters α, β, γ, ξ, c and A of Wrought iron. The calculated values are 1.0832, 15 MPa, 0.0473, 1.36, 12923 MPa and 613 respectively.

4.3 Estimation of accumulated plastic meso-strain

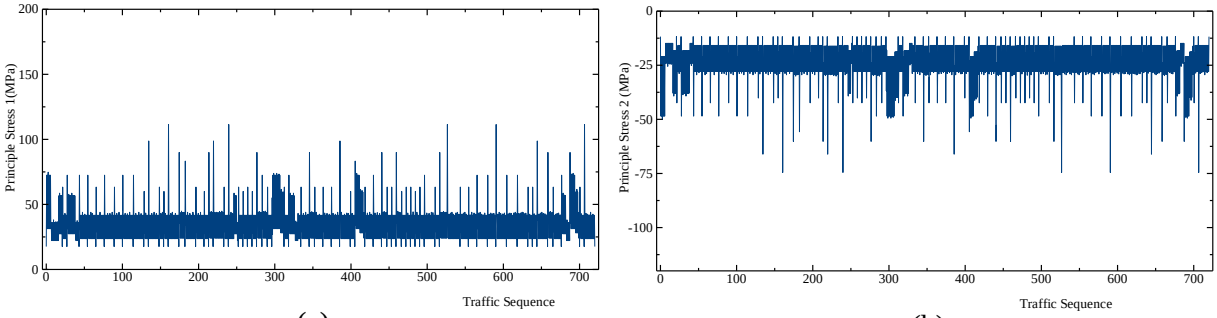

(a) (b)

Figure 9: Principle stress variation with the traffic sequence per single day: (a). Principle stress 1, (b). Principle stress 2

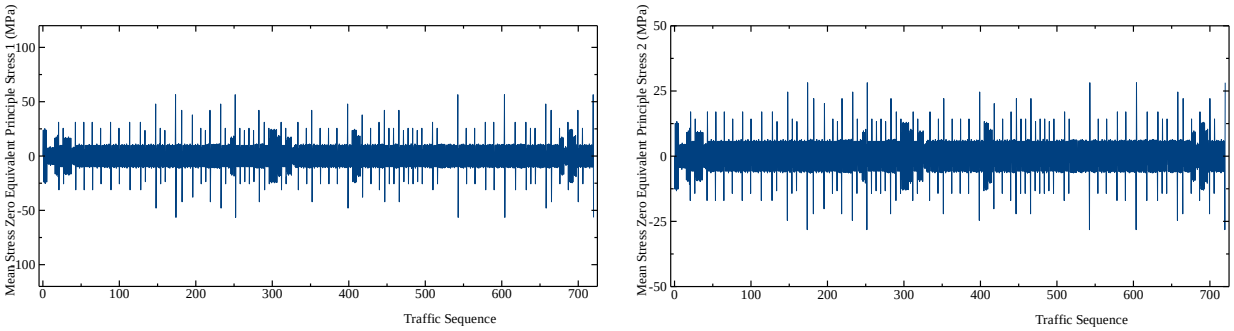

(a) (b)

Figure 10. Mean zero equivalent principle stress variation with the traffic sequence per single day: (a). Principle stress 1, (b). Principle stress 2

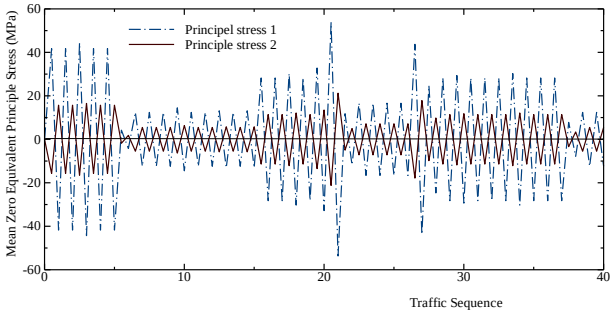

Figure 11. Enlarge fragment of mean zero equivalent principle stresses

The obtained principle stress variations are complex and also of irregular shape (Fig. 9). These stresses should be reduced into a series of equivalent stabilized cycles (zero mean stress cycles) which give the same damage to the material. In order to achieve this goal, initially the famous rainflow cycle counting technique (Suresh, 1998) is used to identify the stress ranges and sequences of closed stress cycles (stress- strain hysteresis loops) (Suresh, 1998; Christ, 1996). Then modified Goodman relation is used to transfer these counted cycle to mean stress zero equivalent stabilized cycle. Some of these transferred principle stresses are plotted in Fig. 10. These figures clearly exhibit that behavior of principle stresses are proportional (see Fig. 11). Finally the accumulated plastic meso-strain per each stabilized cycle is calculated using Eq. (1) and plotted in Fig. 12.

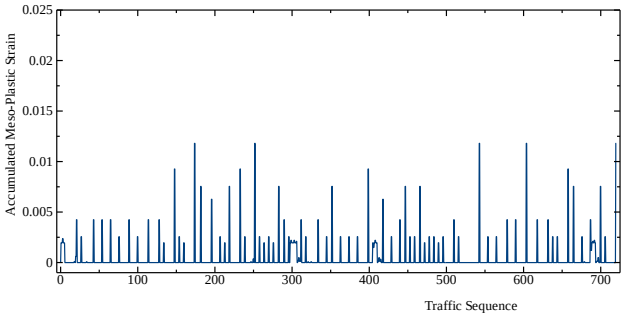

Figure 12. Accumulated meso-plastic strain variation with the traffic sequence per single day

4.4 Fatigue life estimation

The proposed fatigue model in multiaxial fatigue (section 2) was utilized to predict the service life of the riveted connection. The predicted lives are shown in Table 1. Further, it was considered that future sequence and density of rail passage is similar to the present period of operation. The predicted values were also compared with three previous models based estimations (similar approaches considered in section 3) as shown in Table 1. The comparisons revealed that the proposed fatigue model based estimations deviate from previous fatigue theories based estimations.

Table 1: Calculated fatigue lives of riveted connection

Fatigue model	***Fatigue Life (months)***
Effective stress based Miner's Rule (Suresh, 1998)	*1957*
Effective stress based Sequential Law (Mesmeque et al., 2005)	*1315*
Meso-plastic strain based Miner's Rule (Jabbado et al. 2008)	*361*
Meso-plastic strain based proposed model	*294*

5. Conclusions

A new damage indicator based mesoscopic scale fatigue model was proposed. A verification of the new model was conducted by comparing the estimated fatigue life with experimental life under variable amplitude multiaxial proportional loading. The proposed fatigue model was further utilized to estimate the remaining fatigue life of a riveted joint. It was shown that the proposed multiaxial fatigue model gives a much more realistic fatigue life to variable amplitude proporti onal loading situation where detailed stress histories are known. Further applications of proposed model in different connections (i.e. welded and bolted) in offshore steel structures are currently under way.

Acknowledgement

The authors wish to express their sincere gratitude to Professor M.P Ranaweera and the team of experts who worked in the Sri Lankan Railway Bridge project, for their great advice in carrying out this research. Also the authors convey their kind gratitude to Professor E. Macha and Professor Z. Marciniak for providing us with the necessary loading histories and results of multiaxail fatigue tests.

References

Christ, H.J. Cyclic stress-strain response and microstructure. *ASM Hand book*, 19, 1996, 72-95.

Fisher, J.W.; Yen, B.T.; Wang, D. Fatigue and Fracture Evaluation for Rating Riveted Bridges." *NCHRP Report No 302*, Transportation Research Board, National Research Council, Washington D.C, 1994.

Imam, B.; Righiniotis, T.D.; Chryssanthopoulos, M.K. Fatigue assessment of riveted railway bridges. *International Journal of Steel Structures*. 2005, 5(5), 485-494.

Imam, B.M.; Righiniotis, T.D.; Chryssanthopoulos, M.K. Numerical modeling of riveted railway bridge connections for fatigue evaluation. *Engineering Structures*. 2007, 29 (11), 3071-3081.

Jabbado, M.; Maitournam, M.H. A high cycle fatigue life model for variable amplitude multiaxial loading. *Fatigue & Fracture of Engineering Meterials & Structures*. 2008, 31(1), 67-75.

Karolczuk, A.; Macha, E. Fatigue fracture planes and expected principle stress directions under variable amplitude loading. *Fatigue & Fracture of Engineering Materials & Structures*.2005, 28 (1-2), 99-106.

Kluger, K.; Lagoda, T. Application of the Dang-Van criterion for life determination under uniaxial random tension-compression with different mean values. *Fatigue & Fracture of Engineering Materials & Structures*.2004, 27 (6), 505-512.

Marciniak, Z.; Rozumek, D.; Macha, E. Fatigue lives of 18G2A and 10HNAP steels under variable amplitude and random non-proportional bending with torsion loading. *International Journal of Fatigue*. 2008,30 (5), 800-813.

Mesmacque, G.; Garcia, S.; Amrouche, A.; Rubio-Gonzalez, C. Sequential law in multiaxial fatigue, a new damage indicator. *International Journal of Fatigue*. 2005, 27(4), 461-467.

Railtrack. RT/CE/C/025. *Rail track line code of practice: The structural assessment of underbridges*, Railtrack, 2001.

Siriwardane, S.; Ohga, M.; Dissanayake, R.; Taniwaki, K. Application of new damage indicator-based sequential law for remaining fatigue life estimation of railway bridges. *Journal of Constructional Steel Research*. 2008, 64(2), 228-237.

Suresh, S. *Fatigue of materials*; Second edition, Cambridge University Press, UK. 1998.

Troshchenko, V.T.; Shestopal, L.R. Criteria of torsional fatigue strength of metals. *Institute of Strength of Materials, Academy of sciences of Ukrainian SSR*, 1975, 2, 127-131.